How to cite: Angew. Chem. Int. Ed. 2025, e202418054
doi.org/10.1002/anie.202418054

Enzyme Catalysis

Mechanistic Insights Into Post-Translational α-Keto-β-Amino Acid Formation by a Radical *S*-Adenosyl Methionine Peptide Splicease

Anna L. Vagstad, Edgars Lakis, Katja-Sophia Csizi, William Walls, Daniel Richter, Kang Soo Lee, Roman Stocker, Muriel Gugger, William E. Broderick, Joan B. Broderick, Markus Reiher, and Jörn Piel**

Abstract: Radical *S*-adenosyl methionine enzymes catalyze a diverse repertoire of post-translational modifications in protein and peptide substrates. Among these, an exceptional and mechanistically obscure example is the installation of α-keto-β-amino acid residues by formal excision of a tyrosine-derived tyramine unit. The responsible spliceases are key maturases in a widespread family of natural products termed spliceotides that comprise potent protease inhibitors, with the installed β-residues being crucial for bioactivity. Here, we established the in vitro activity of the model splicease PcpXY to interrogate the mechanism of non-canonical protein splicing. Identification of shunt and coproducts, deuterium labeling studies, and density functional theory energy calculations of hypothesized intermediates support a mechanism involving hydrogen abstraction at tyrosine Cα as the initial site of peptide radical formation and release of 4-hydroxybenzaldehyde as the tyrosine-derived coproduct. The data illuminate key features of this unprecedented radical-mediated biotransformation yielding ketoamide pharmacophores that are also present in peptidomimetic therapeutics.

[*] A. L. Vagstad, E. Lakis, D. Richter, J. Piel
Institute of Microbiology, Eidgenössische Technische Hochschule (ETH) Zürich, 8093 Zurich, Switzerland
E-mail: avagstad@ethz.ch
jpiel@ethz.ch

K.-S. Csizi, M. Reiher
Institute of Molecular Physical Science, Eidgenössische Technische Hochschule (ETH) Zürich, 8093 Zurich, Switzerland

W. Walls, W. E. Broderick, J. B. Broderick
Department of Chemistry & Biochemistry, Montana State University, 59717 Bozeman, Montana, United States

K. Soo Lee, R. Stocker
Department of Civil, Environmental and Geomatic Engineering, Eidgenössische Technische Hochschule (ETH) Zürich, 8093 Zurich, Switzerland

K. Soo Lee
Department of Mechanical Engineering, Ulsan National Institute of Science and Technology (UNIST), 44919 Ulsan, South Korea

M. Gugger
Institut Pasteur, Université Paris Cité, Collection of Cyanobacteria, F-75015 Paris, France

Introduction

α-Keto-β[3]-amides (from here referred to as ketoamides) are pharmacophores of various peptidomimetic drugs and drug candidates that inhibit serine and cysteine proteases (Figure 1a).[1] Examples are the clinically used narlaprevir **1** that blocks hepatitis C virus protease,[2] as well as potent inhibitors of coronaviral proteases.[3] In addition to these synthetic compounds, some non-ribosomally synthesized natural peptides contain ketoamides, such as the trypsin inhibitor cyclotheonamide A **2**.[4–7] Through genome mining and heterologous expression, we previously discovered a family of post-translational modification enzymes that introduce ketoamide moieties into the α-amino acid backbones of ribosomally synthesized peptides and proteins.[8] These enzymes belong to the radical *S*-adenosyl methionine (rSAM) superfamily[9] and act on XYG motifs (X being a variable residue) to catalyze a remarkable splicing reaction involving net tyramine excision (Figure 1b). Reconnection of the peptide backbone forms a new C–C bond to elongate residue X with the remaining tyrosine-derived C1 carbonyl unit. The resulting ketoamide residues with variable side chains are the defining feature of a large microbial family of ribosomally synthesized and post-translationally modified peptide (RiPP) natural products termed spliceotides.[10] Bioassays with three select spliceotides revealed all of them as potent protease inhibitors. The CyiA spliceotide **3**, for example, exhibited low nanomolar inhibition of neutrophil elastase, a drug target for inflammatory diseases.[10,11] Furthermore, the splicing reaction has been utilized for protein engineering, with the installed chemically unique α-keto functionality serving as a target site for bioorthogonal labeling.[12,13]

RiPPs are matured by post-translational modification of the core region of a gene-encoded precursor.[14] Proteolytic cleavage then releases the mature core from its N-terminal leader (or other recognition elements) to yield the peptide natural product, often concomitant with export outside the cell. In addition to spliceases, rSAM maturases from RiPPs catalyze a myriad of post-translational modifications—including installation of C–C or C–heteroatom cross-links, D-amino acids, and methyl groups—resulting in a large structural and functional diversity.[14] In canonical rSAM catalysis, SAM is reductively cleaved by a coordinating [4Fe–4S] cluster to yield a reactive primary 5'-deoxyadenosyl radical (dAdo•), which abstracts a substrate hydrogen to

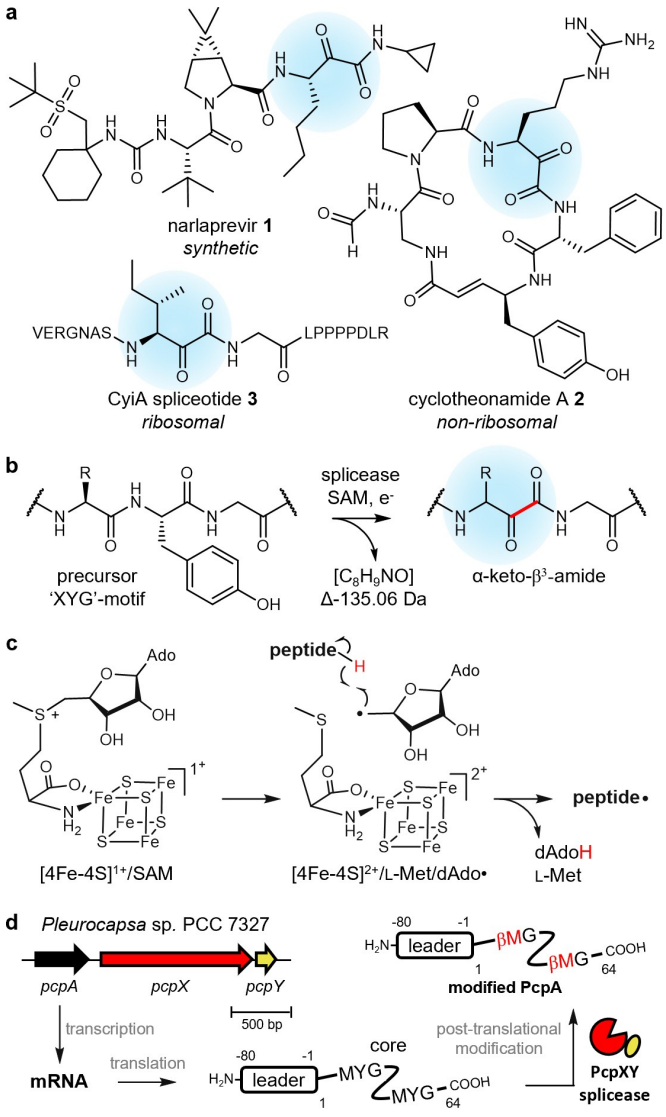

Figure 1. Post-translational spliceases modify ribosomally translated precursor proteins. a) A synthetic drug and representative peptide natural products containing the protease-inhibiting ketoamide pharmacophore, highlighted in blue. b) Spliceases catalyze the net excision of tyramine at XYG splice sites. The new bond formed between the C1 of residue X and C1 of the former tyrosine is shown in red. The stereochemistry of the β-amino acid was not determined in this study but was detected as a mixture of the D- and L-isomers from previous coexpression experiments.[8] This position is prone to racemization due to the electrophilicity of the neighboring carbonyl.[1] c) Canonical radical initiation mechanism of peptide-modifying rSAM enzymes. d) The type I splicease biosynthetic gene cluster pcp encoding a Nif11-type precursor (PcpA) containing two MYG splice sites, the splicease (PcpX), and an accessory protein (PcpY) essential for splicing. SAM; *S*-adenosyl methionine. βM; the β-amino acid residue product of Met. dAdo•; 5'-deoxyadenosyl radical. dAdoH; 5'-deoxyadenosine.

initiate the reaction (Figure 1c).[9,15] This [4Fe–4S] cluster is bound by the cysteine thiols of a conserved CX_3CX_2C motif within the rSAM domain (Pfam entry PF04055). Many peptide-modifying rSAM enzymes, including the spliceases, additionally contain a C-terminal SPASM domain (PF13186) that harbors two auxiliary [4Fe–4S] clusters bound by 7–8 cysteine residues.[16,17] In the case of only seven cysteines, the open iron-coordination site is thought to be important for substrate binding and catalysis.

No precedent exists in nature or synthetic chemistry for the elaborate and as-yet uncharacterized backbone bond breaking and making reactions of spliceases, presenting an intriguing target for mechanistic studies. Here, we established the in vitro activity of the representative type I splicease PcpXY from a cyanobacterium (Figure 1d). Characterization of shunt metabolites and coproducts, deuterium-labeling studies, and energy calculations of projected intermediates allowed us to propose a mechanistic hypothesis for splicease catalysis. Insights garnered from these studies expand the knowledge of the diverse reaction paths accessible to rSAM enzymes and might also inspire new methodology in organic synthesis.

Results and Discussion

Establishment of in Vitro Splicease Activity

rSAM enzymes are inherently challenging to work with in vitro due to their oxygen-sensitive iron-sulfur clusters. For this study, we selected five pathways for protein production and solubility screens (Table S1–S4). The pathways belong to the initially discovered type I spliceotide family from cyanobacteria[8] and comprise one or several Nif11 type precursors (designated protein A), the splicease (protein X), and an essential accessory protein (protein Y). Eleven types of spliceotide biosynthetic gene clusters from diverse bacteria and some archaea have been identified to date.[10] Types are differentiated by the phylogeny of the splicease and the class of precursor protein substrate. The Nif11 precursor leaders derive their name from similarity to a nitrogen fixation-associated protein and are also found in other RiPP families.[18] The accessory Y proteins are uniquely found in the type I spliceotide pathways and are hypothesized to serve as RiPP recognition elements (RREs)[19] that mediate protein–protein interactions between the precursor leader and the splicease. Expression tests in *E. coli* indicated that the *pcp* pathway from *Pleurocapsa* sp. PCC 7327[20] yielded N-terminally His_6-tagged proteins with the best overall yields and good aerobic stabilities (Figure S1). The PcpA precursor contains a 64-amino-acid core with two MYG motifs at Tyr15 and Tyr56 (Figure 2a), which were previously shown to be the targets of the PcpXY splicease in *E. coli* heterologous expression experiments.[8]

To conduct in vitro assays, PcpX (alone or together with PcpY) and PcpA were heterologously produced in *E. coli* BL21(DE3) and aerobically purified by Ni^{2+}-affinity column chromatography (Figure S2). Fusion of PcpX to a SUMO solubility tag[21] improved protein yields and was used in later experiments. The [4Fe–4S] clusters of PcpX were reconstituted anaerobically and the *holo* enzyme used for in vitro reactions. PcpA core peptide fragments were detected by liquid chromatography–high-resolution mass spectrometry (LC-HRMS) following protease digest (Table S5). Small

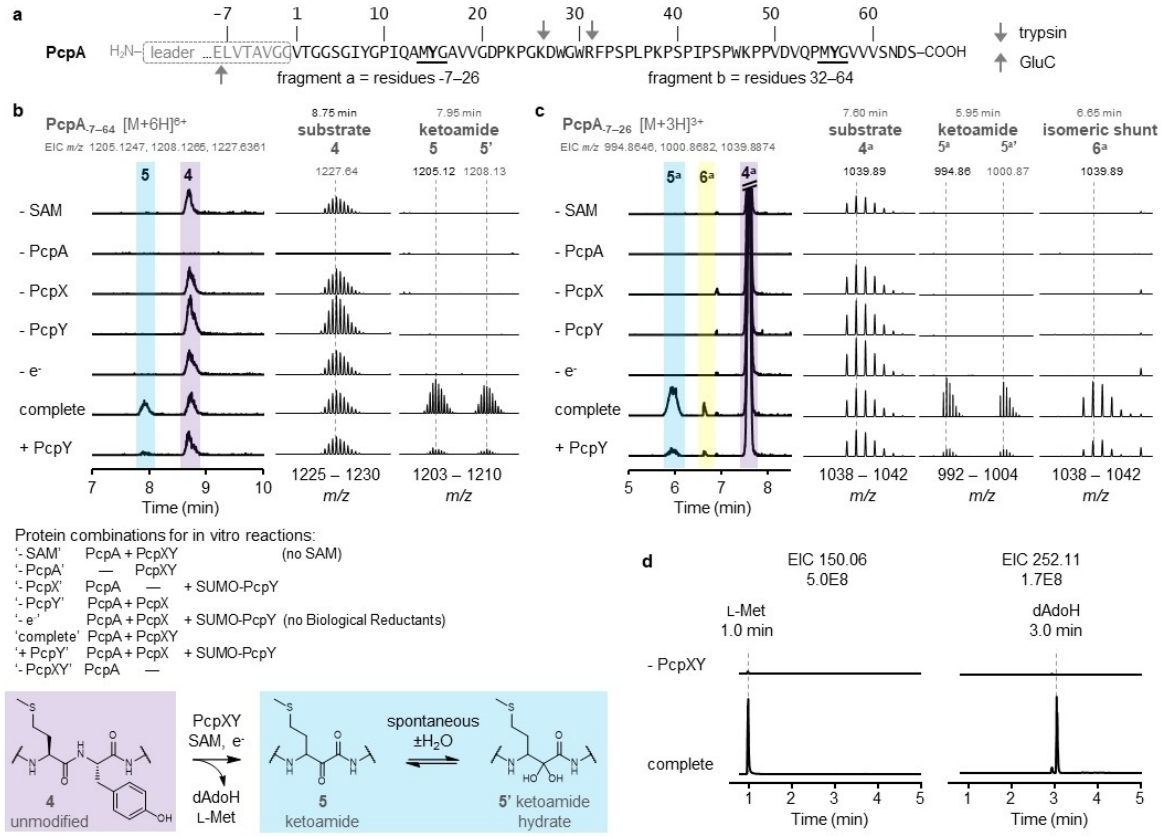

Figure 2. In vitro splicease activity detected by LC-HRMS. a) Partial sequence of the PcpA precursor containing the relevant C-terminal core fragments. Splice sites at Tyr15 and Tyr56 are underlined. Extracted ion chromatograms (EICs) for the substrate and product peptide fragments for b) GluC-released $PcpA_{-7–64}$ and c) GluC and trypsin-released $PcpA_{-7–26}$ (superscript 'a'). Only trace amounts of ketoamide product were detected for the $PcpA_{32–64}$ peptide fragment (see Figure S3). Ion counts are normalized within each panel. Protein combinations for each reaction are as described using the biological reductant system (FldA, Fpr, and NADPH) as the electron source and SAM as the cosubstrate. Reactions additionally contain dithiothreitol (DTT). Structures of the peptide substrate and ketoamide products are shown for the net splicease reaction (lower left). d) Detection of L-Met and dAdoH splicease coproducts for the complete reaction relative to the negative control lacking PcpXY.

molecule products were directly detected from acid-quenched reactions by LC-HRMS. The in vitro methods developed in this paper were used in a parallel study to examine the role of a structurally conserved helix from the Y proteins.[22]

Overnight reactions were digested with glutamyl endopeptidase (GluC) to release the peptide fragment corresponding to PcpA residues −7 to 64 ($PcpA_{-7–64}$), where position 1 refers to the start of the core following the native Gly-Gly baceriocin-type cleavage motif.[23] In addition to a peptide fragment derived from the unmodified substrate **4**, we detected another Δ-135.06 Da peptide product **5**, consistent with ketoamide formation at one of the two possible splice sites (Figure 2b). The ketoamide peptide is detected as a mixture with its α-ketone hydrate **5′** resulting from water addition. Separation of the PcpA splice sites by additional cleavage with trypsin to release $PcpA_{-7–26}$ and $PcpA_{32–64}$ confirmed Tyr15 as the preferred splice site with only trace amounts of modified Tyr56 evident (Figure 2c, Figure S3). In some efficient reactions, a doubly modified $PcpA_{-7–64}$ Δ-270.12 Da species was detected (Figure S4). In addition to the spliced products, we also detected a new peptide **6** that was equivalent in mass to the substrate, suggesting it is an isomerized shunt product. Whereas the ketoamide **5** was already abundant after 15 min and maximally produced after approximately 2 h, the isomer **6** predominantly accumulated at later timepoints (Figure S5).

As expected, controls demonstrated that PcpA, PcpX, PcpY, SAM, and reductant were essential reaction components. Inclusion of dithiothreitol (DTT) improved yields, and the biological reductant system [i.e., flavodoxin (FldA), flavodoxin reductase (Fpr), and nicotinamide adenine dinucleotide phosphate (NADPH)] was more effective than chemical reductants (i.e., sodium dithionite and methyl viologen) to generate spliced products (Figure S6). Reactions with PcpX expressed alone were complemented by addition of SUMO-tagged PcpY ('+PcpY' sample, Figure 2b–c, Figure S3). Furthermore, untagged PcpY co-elutes with His_6-tagged PcpX purified by Ni^{2+}-affinity column chromatography (Figure S7) and provision of extra PcpY to the 'complete' set of reaction components did not improve conversion (Figure S8), indicating PcpX and PcpY form a stable protein complex. We also recently reported that PcpA substrate binding is mediated by the presence of PcpY, as shown by size exclusion chromatography and AlphaFold modeling of the PcpAXY complex.[22]

The reductive cleavage products of SAM, 5'-deoxyadenosine (dAdoH) and L-methionine, accumulated in reactions as coproducts (Figure 2d). Thus, SAM appears to act as a substrate rather than a regenerated cofactor, in line with other studies on peptide-modifying rSAMs.[24] Initially, no small-molecule products associated with the lost tyramine unit could be identified.

Spectroscopic Characterization of Reconstituted PcpXY

Next, we assessed the spectroscopic properties of the splicease and its iron-sulfur clusters. PcpXY was purified aerobically and buffer-exchanged to deoxygenated buffer in an anaerobic chamber. A sample of this as-purified PcpXY was retained and compared to the reconstituted enzyme regarding in vitro activity and iron and sulfide content (Figure S9). As-purified PcpXY contained 5.15 ± 0.02 Fe and 6.08 ± 0.19 S^{2-}, consistent with one intact [4Fe–4S] cluster being present on average. Upon reconstitution, iron and sulfide content increased to 13.6 ± 1.5 and 11.7 ± 0.4, respectively, and the protein developed a prominant UV/Vis absorption band at 410 nm, suggesting three intact [4Fe–4S] clusters are present, as expected for rSAM-SPASM enzymes. Only a trace amount of the ketoamide product was observed for the as-purified splicease, while the reconstituted enzyme produced the ketoamide peptide as described in the previous section.

Reconstituted PcpXY was further characterized by electron paramagnetic resonance (EPR) spectroscopy. The as-reconstituted protein is primarily EPR silent, exhibiting only a small signal with g-values indicative of a $[3Fe–4S]^{+}$ cluster (Figure S10).[25] Reduction of PcpXY with dithionite yields a composite spectrum composed of multiple overlapping signals (Figure 3). All component signals exhibit temperature-relaxation (Figure S11) and power saturation (Figure S12) behavior consistent with their assignment to $[4Fe–4S]^{+}$ clusters.[26] Addition of SAM to reduced PcpXY significantly perturbed one of the component signals, as evidenced most clearly by the reduced intensity of the $g = 2.018$ feature and the appearance of a new feature at $g = 1.868$. The perturbation of primarily one signal is consistent with SAM coordination to the unique iron of the rSAM [4Fe–4S] cluster, as occurs in a wide range of rSAM enzymes.[9] Addition of SAM also leads to an overall sharpening of signals and the resulting observation of previously unresolved features. While SAM is not expected to directly interact with the iron-sulfur clusters of the SPASM domain, sharpening of the EPR spectrum suggests that SAM binding has structural implications beyond the rSAM cluster.

Deuterium Labeling Studies Define the Site of Initial H-Abstraction

We then considered which hydrogen is abstracted by dAdo• to initiate catalysis. PcpA variants were differentially labeled with deuterium at the conserved YG of splice sites, and

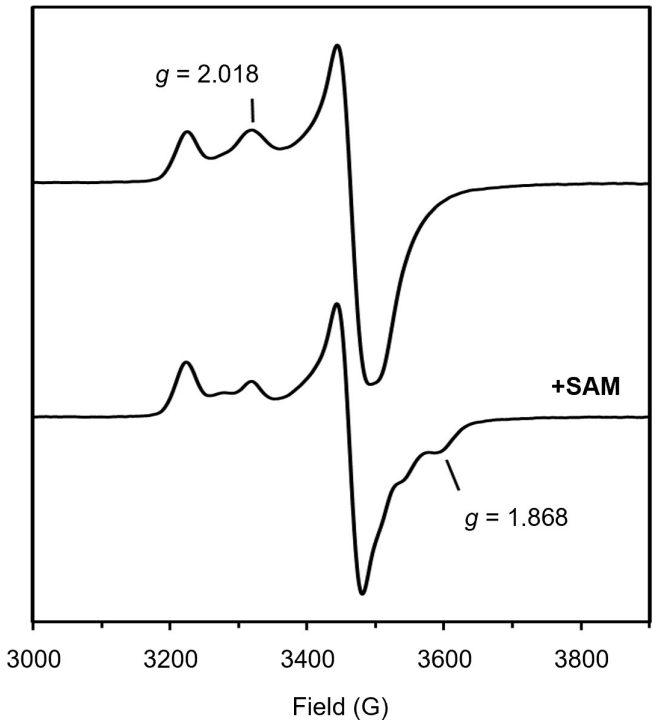

Figure 3. X-band EPR spectra of reconstituted and sodium dithionite–reduced PcpXY in the presence and absence of SAM. EPR conditions: microwave frequency, 9.38 GHz; microwave power, 0.1 mW; modulation, 10 G; and T = 10 K.

transfer of the label to dAdoH was assessed by LC-HRMS analysis of in vitro reactions. The PcpA variants were obtained by individually feeding the commercially available amino acids ($^{2}H_{7}$)-Tyr, (3,3-$^{2}H_{2}$)-Tyr, and (2,2-$^{2}H_{2}$)-Gly in minimal medium expressions and purifying the resulting precursors (Figure S13). Reactions in deuterium oxide were additionally conducted to test whether an exchangeable hydrogen—for example, at the phenol oxygen of tyrosine or of the amide nitrogens—was involved in H-abstraction. The *m/z* 253.12 ion corresponding to $[M+H]^{+}$ dAdoD (i.e., dAdoH with one ^{2}H label) was only enriched for overnight reactions with ($^{2}H_{7}$)-Tyr-labeled PcpA and in deuterium oxide (Figure S14). Monitoring of reaction timepoints in deuterium oxide showed only a delayed accumulation of the dAdoD product that did not correspond to the early formation of the ketoamide, demonstrating it arises from a shunt process (Figure S15). Thus, the results support the Cα of tyrosine as the probable site of initial H-abstraction.

To further probe the importance of this site, (2-^{2}H)-L-Tyr was enzymatically synthesized from L-Tyr in deuterium oxide by the tryptophanase TnaA[27] and incorporated by feeding into PcpA (Figure S16). To avoid depletion of the Cα-deuterium label by reversible transamination, the quintuple transaminase mutant strain *E. coli* Δpenta[28] was used as expression host. In vitro reactions cleanly showed Cα-deuterium abstraction from this substrate to produce dAdoD concomitant with formation of the ketoamide **5** in early timepoints (Figure 4a–b, Figure S17). The orthogonally labeled substrate was predominantly produced by feeding

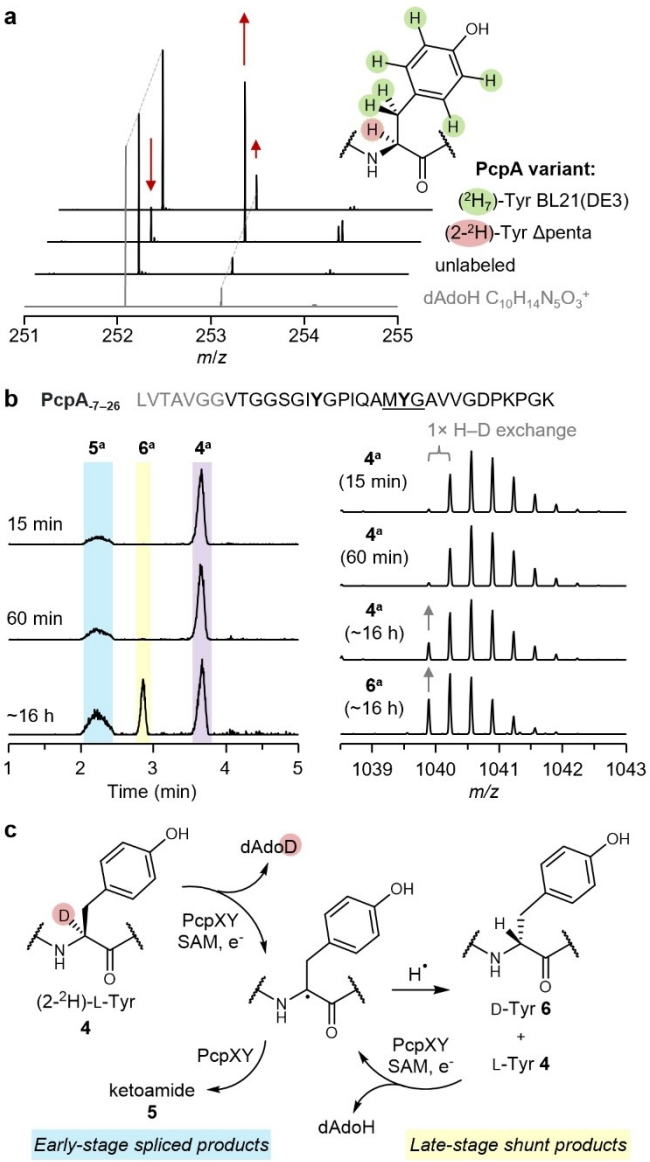

Figure 4. Deuterium-labeling studies of in vitro splicease reactions. a) Mass spectra of dAdoH/D products detected from reactions with deuterium-labeled PcpA substrate variants relative to the unlabled control (60 min timepoint). The dAdoD product at *m/z* 253.12 accumulates in the (2-^{2}H)-Tyr PcpA substrate produced in the transaminase deletion strain *E. coli* Δpenta. Note that the Cα deuterium of the fed ($^2H_7$)-Tyr is depleted by reversible transamination in BL21(DE3) to yield predominantly ($^2H_6$)-Tyr-labeled PcpA. The simulated mass spectrum of dAdoH with natural isotope abundance is shown for comparison. b) LC-HRMS analysis of the (2-^{2}H)-Tyr PcpA substrate reaction. EICs for the substrate and product peptide fragments for $PcpA_{7–26}$ released by GluC and trypsin digest are shown (left). Only the spliced ketoamide **5** was detected in the early timepoints at 15 and 60 min. Mass spectra (right) show the depletion of the deuterium label from substrate **4** at 16 h concomitant with formation of the H–D exchanged isomeric shunt **6**. c) Rationale for accumulation of unlabeled dAdoH and H–D exchanged **4** at later timepoints of the (2-^{2}H)-Tyr PcpA reaction.

($^2H_7$)-Tyr in a BL21(DE3) host where the Cα-deuterium was highly depleted through transaminase-mediated exchange with hydrogen (Figure S13). As expected, this orthogonally labeled substrate gave only minimal enrichment of dAdoD (Figure 4a, Figure S17). From this data, we infer that a single equivalent of SAM is utilized in the reaction to the spliced product. Logic dictates that if another equivalent of SAM had been involved in abstraction of a second hydrogen during ketoamide formation, we would have observed an equal amount of AdoH and dAdoD in the 15 and 60 min timepoints for the (2-^{2}H)-Tyr-PcpA reaction since only a single deuterium is present per splice site. The low amount of dAdoH for this substrate also supports that nonproductive turnover of SAM (i.e., accumulation of dAdoH through spontaneous quenching of dAdo•) is minimal at early timepoints.

Analysis of the peptide products from the (2-^{2}H)-Tyr-labeled PcpA reaction timecourse revealed that both the starting material **4** and its isomeric shunt product **6** lost a Cα deuterium label in the extended 16 h timepoint (Figure 4b). We hypothesize that the Tyr-Cα• intermediate may be spontaneously quenched in a shunt reaction to give an epimeric mixture of the L- and D-Tyr. In H_2O, these species would incorporate a hydrogen from the protein or another reaction component. The newly labeled L-Tyr substrate **4** would then be subject to hydrogen abstraction to give dAdoH (Figure 4c). The dAdoH may additionally arise from uncoupled turnover of SAM, which may occur more frequently in later reaction timepoints as the L-Tyr peptide substrate is depleted.

Characterization of Shunt Metabolites Informs the Splicease Mechanism

To test the hypothesis that the isomeric product **6** is the D-Tyr shunt, the core peptide from a scaled-up in vitro reaction using conditions that favored accumulation of **6** was subjected to advanced Marfey's analysis (Figure S18).[29] The hydrolyzed and derivatized amino acid monomers were separated by LC-HRMS and compared to similarly derivatized L- and D-Tyr standards and hydrolysates of the unmodified PcpA core peptide isolated from a negative-control reaction lacking SAM. A clear signal for D-Tyr not present in the negative control confirmed the identity of **6** as the D-Tyr epimer (Figure 5a).

During early struggles with inconsistent in vitro splicease activity, no small-molecule products related to the excised tyramine could be detected. We therefore performed a broader LC-HRMS-based metabolomics analysis of culture extracts from *E. coli* expressions of several splicease systems to search for cryptic coproducts. Several reaction products were identified that contributed to our understanding of splicease catalysis. Samples from the *Thiothrix nivea* DSM 5205 type III spliceotide containing four splice sites[10] revealed 4-hydroxybenzaldehyde **7** (*m/z* 121.03) as a putative tyrosine side-chain product (Figure S19). In follow-up experiments, in vitro reactions with PcpA partially labeled with ($^{13}C_9$)-Tyr (Figure S13) demonstrated PcpXY-dependent formation of **7** enriched with seven ^{13}C labels (*m/z* 128.05, Figure 5b), which accounts for the entire tyrosine

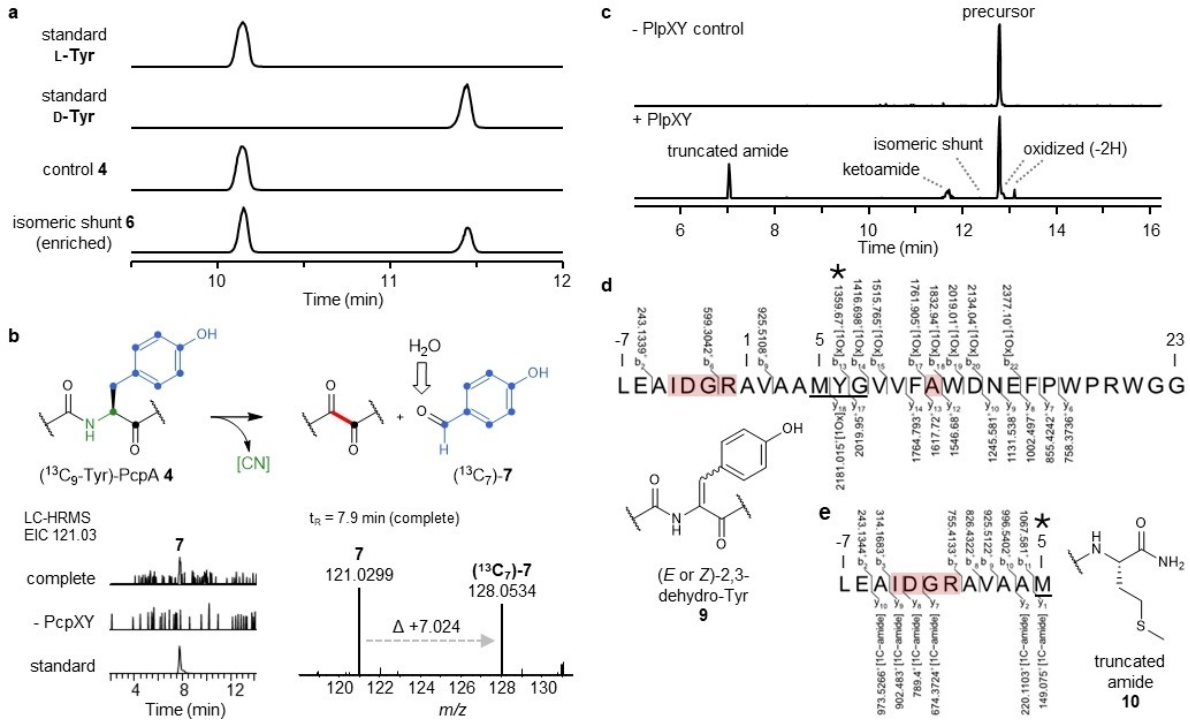

Figure 5. Detection of shunt metabolites and coproducts from splicease reactions. a) Marfey's analysis of $PcpA_{1–64}$ core peptide hydrolysates from an in vitro reaction favoring production of the isomeric shunt **6** compared to a '−SAM' control reaction and L- and D-Tyr standards. EICs for the bis-N-α-(2,4-dinitro-5-fluorophenyl)-L-valinamide (L-FDVA) derivatized Tyr are shown, $[M-H]^-=740.23$. b) LC-HRMS analysis of the 4-hydroxybenzaldehyde **7** side chain coproduct of the PcpA ketoamide-forming in vitro reaction. Mass spectra of in vitro reactions with ($^{13}C_9$)-Tyr-label-enriched PcpA produced a mixture of unlabeled, $[M-H]^-=121.03$, and $^{13}C_7$-labeled, $[M-H]^-=128.05$, **7**. c) Identification of shunt products from a Plp spliceotide mutant produced in *E. coli*. Coproduction of the His_6-tagged PlpA3 mutant with its cognate splicease ('+PlpXY') compared to the precursor only control ('−PlpXY'). LC-HRMS analysis of Ni^{2+}-affinity column chromatography purified precursor cleaved with GluC. Non-native residues are highlighted in red where 'IDGR' is a factor Xa (fx) recognition site substitution and P11A is a proline-to-alanine point mutant at core residue 11. EICs for the precursor/isomeric shunt $[M+3H]^{3+}=1127.55$, ketoamide $[M+3H]^{3+}=1082.53$, oxidized $[M+3H]^{3+}=1126.88$, and truncated amide $[M+2H]^{+2}=608.33$ are shown. d) MS^2 analysis of the *m/z* 608.33 feature at 13.1 min localized the −2 Da mass shift ('1Ox'-labeled fragment ions) to the Tyr6 residue. Oxidized peptide species are predicted to correspond to the *E* and *Z* isomers of **9**. e) MS^2 analysis of the *m/z* 608.33 feature at 7.1 min localized the amide to Met5 ('1C-amide'-labeled fragment ions) of the truncated peptide and is proposed to correspond to structure **10**. Asterisks indicate the modified residue.

side chain and leaves only the backbone-derived C2 and N1 unaccounted for. Thus, the excised part is likely not expelled as intact tyramine but rather broken apart.

Consequently, we predicted several other small molecules as possible coproducts that might contain the remaining backbone-derived atoms, such as cyanide or formaldehyde. The presence of these small molecules was probed by derivatizations with selectively reactive agents and detection by LC-HRMS or Surface-enhanced Raman spectroscopy (SERS).[30] These methods were validated by spiking control reactions with small-molecule standards. Derivatization of splicease reactions with 2,3-napthalenedicarboxaldehyde[31] or 2,4-dinitrophenylhydrazine[32] gave no detectable cyanide or formaldehyde product ions, respectively, by LC-HRMS. Furthermore, a cyanide signal[33] was not found from the SERS measurement. Thus, the fate of the remaining C2 and N1 from the substrate tyrosine is still under investigation after extensive trials.

Other shunt metabolites were identified in various coexpressions of the type I *plp* splicase (Figure 5c, Figure S20). His_6-tagged PlpA3-P11A mutant precursor coproduced with PlpXY gave two peptide species corresponding to the loss of two hydrogens, with the -2.016 Da mass change localized to the substrate tyrosine residue by MS^2 fragmentation for the more abundant species eluting at 13.1 min (Figure 5d). These minor side products might be the *E* and *Z* forms of 2,3-dehydrotyrosine **9**, resulting from an oxidation of the tyrosine side chain directly or via a *p*-quinone methide **8** intermediate, which is expected to rapidly tautomerize to **9**. As a parallel example of oxidized species resulting from radical-mediated catalysis, aromatic 2,3-dehydroamino acid residues were proposed as shunt products of the $C(sp^2)$–$C\beta(sp^3)$ crosslinking rSAM-SPASM enzymes from triceptide and daropeptide RiPP biosynthesis.[34,35] We also observed a truncated species corresponding to cleavage between the N1 and C2 of tyrosine to give a terminal amide **10** (Figure 5e). The truncated amide was noted in our previous *plp* study[8] and could arise from hydrolysis of **9**[36] or be a decomposition product of the Cα radical intermediate (Figure S20). Peptide Cα radicals are known to react with oxygen to give a

hydroxylated Cα species that rapidly degrades to the favored N-terminal amide and C-terminal carbonyl fragments.[37] Neither the amide cleavage product nor the putative dehydrotyrosine species were detected from anaerobic in vitro reactions with the Pcp system.

Thermodynamic Analysis of Mechanistic Proposals for the Splicease Reaction

Collectively, the results support the following mechanistic aspects: (i) Cα of tyrosine in the XYG motif is the site of initial H-abstraction to form the radical intermediate $\mathbf{R1_{red}}$, (ii) quenching of this intermediate with hydrogen regenerates the substrate or forms the D-Tyr **6** shunt product, (iii) 4-hydroxybenzaldehyde **7** from the tyrosine side chain is one of the splice products, and (iv) tyrosine side-chain oxidation occurs either as a side reaction or during splicing. Note that we use the subscripts 'red' and 'ox' to denote if the species contains the unmodified tyrosine or the oxidized quinone methide side chain, respectively. Since the splicing reaction occurs anaerobically, the oxygen atom of **7** is most likely derived from water. A mechanistic rationale that would account for the aldehyde oxygen, the dehydrotyrosine byproduct **9**, and the undetected N1 and C2 atoms of tyrosine is shown in Figure 6a. The dehydrotyrosine radical moiety $\mathbf{R1_{ox}}$ would be the precursor of an extruded 7-cyano *p*-quinone methide $\mathbf{P_{ox}}$. Spontaneous addition of water then results in the cyanohydrine **11** that decomposes to the verified aldehyde **7** and a cyanide anion. This spontaneous chemistry has precedence in the degradation of plant cyanogenic glycosides such as dhurrin.[38] Furthermore, we found that commercially acquired **11** rapidly degrades to **7** under our reaction conditions (Figure S21). Although extensive analytical efforts did not detect cyanide, it may be consumed by reacting with other assay components, such as sulfur centers in the splicease or flavodoxin, or splicease iron centers.[39]

We considered various hypotheses for the early reaction steps stemming from the experimentally verified Tyr-Cα• $\mathbf{R1_{red}}$. A possible route involved side-chain oxidation to the quinone methide radical $\mathbf{R1_{ox}}$, perhaps mediated by the auxiliary [4Fe–4S] clusters. From here, two alternative mechanisms are proposed: In Pathway A, intermediate $\mathbf{A\text{-}I_{ox}}$ undergoes fragmentation and 1,3 migration of an acyl radical to yield intermediate $\mathbf{R2_{ox}}$ with the formative backbone C–C bond in place. Fragmentation of $\mathbf{R2_{ox}}$ would then generate the ketoamide **5** and the cyano quinone methide $\mathbf{P_{ox}}$ upon oxidation. In Pathway B, an alternative rearrangement involving a cyclic transition state is considered. In the first differential step, $\mathbf{R1_{ox}}$ undergoes cyclization to the azetine transition state $\mathbf{B\text{-}I_{ox}}$. The azetine decomposes via $\mathbf{R2_{ox}}$ into the cyano quinone methide $\mathbf{P_{ox}}$ and the peptide radical, which is oxidized to the ketoamide **5** as in Pathway A. In both pathways, we hypothesized that intermediates might be held in a favorable conformation by iron chelation at the open coordination site of the auxiliary I cluster.

To gain preliminary insights into the feasibility of these mechanistic proposals, we evaluated energies of structures for the presumed intermediates of the alternative pathways applying density functional theory (Figure 6b–c). Additional calculations of activation barriers for the proposed reaction trajectories were not considered at this time. We employed a simplified structural model of the XYG motif where X is glycine, a confirmed substrate of the Plp splicease.[13] All reactions were analyzed for both the unmodified ('red') and the oxidized quinone-methide ('ox') tyrosine side-chain variants, since the explicit oxidation state could not be definitively assigned. The calculated electronic energies and Cartesian coordinates are given in Table S6 and Tables S7–S17, respectively.

We found that initial H-abstraction at the Tyr-Cα of **4** by dAdo• is thermodynamically favored by at least −81 kJ/mol to form $\mathbf{R1_{red}}$ (Figure 6b–c). Subsequent formation of intermediate **A-I** (Pathway A, Figure 6b) via C–N bond cleavage, however, is thermodynamically constrained. This is likely due to poor resonance stabilization of the unpaired electron in the acyl radical. We therefore probed the role of the auxiliary I [4Fe–4S] cluster as a catalyst.[40] Species involving iron coordination are indicated by '@4Fe4S' superscript. For the [4Fe–4S] cubane, we find consistent antiferromagnetic coupling of two pairs of iron atoms for all steps evaluated in this work, which is in agreement with previous studies on related clusters.[41] We assessed conversion of **R1** to **A-I** involving a [4Fe–4S] cubane proceeding either through formation of the acyl radical and subsequent coordination to the vacant metal site, or vice versa (Figure S22). Coordination of **R1** to the vacant iron site provides a thermodynamic sink, where bidentate O–O coordination is found (Figure 6c and S22). This sink is more exothermic for the quinone methide variant. Thus, iron coordination of **R1** followed by fragmentation to **A-I** appears to be the favored route for intermediates from Pathway A. The subsequent C–C bond formation to yield the iron-coordinated species $\mathbf{R2^{@Fe4S4}}$ is almost thermoneutral for the tyrosine side chain and only slightly endothermic for the quinone methide variant but could occur spontaneously under standard conditions.

As an alternative to the 1,3-acyl migration of Pathway A, the **R1** to **R2** transition could proceed via the azetine 4-ring transition state **B-I** depicted in Pathway B. Efforts to calculate the potential energy surface of the **B-I** molecule failed to find a local minimum, limiting our ability to access the feasibility of Pathway B with our simplified model. Following the $\mathbf{R2^{@Fe4S4}}$ intermediate, subsequent dissociation of the side chain and abstraction of a hydrogen equivalent would form [4Fe–4S]-bound $\mathbf{5^{@Fe4S4}}$ and **P** in an exothermic reaction step. Ultimately, dissociation of the ketoamide product to recover the iron-catalyst is only slightly endothermic. Figure 6c shows the general effect of iron-coordination for the shared intermediates between Pathways A and B. Note that we consider dissociation of the product in a dispersion-free environment (i.e., in vacuo). The accurate description of dispersion effects inside the protein cavity might further stabilize the dissociation.

For the overall pathway, we find analogous thermodynamic trends for both side-chain variants (i.e., tyrosine and quinone methide); however, the spontaneous addition of

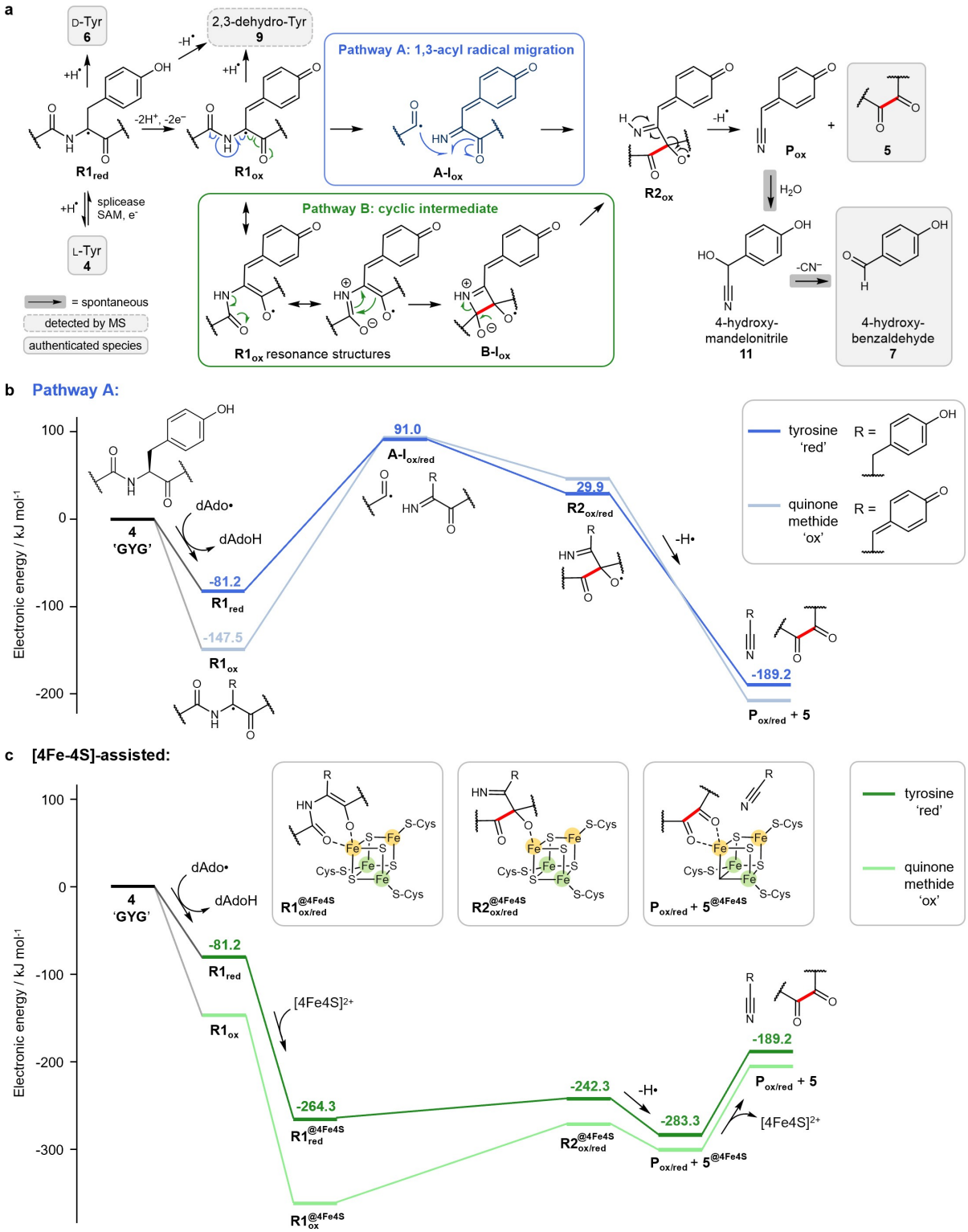

Figure 6. Mechanistic proposals for the splicease reaction. a) Alternative proposals to the ketoamide are shown with the critical new C–C bond in red with side-chain oxidation to the quinone methide. $\mathbf{P}_{ox}$ spontaneously degrades to the verified side-chain coproduct **7**. Thermodynamic reaction profiles are shown for both the tyrosine ('red' subscript) and oxidized quinone methide ('ox' subscript) side chains in the modeled 'GYG' motif for b) the 1,3-acyl radical migration of Pathway A and c) the [4Fe–4S]-assisted conversion of **R1** to the products. It was not possible to calculate an energetic minimum for the proposed intermediate **B**–**I**. Reaction steps involving the proposed auxiliary I open Fe coordination site as catalyst are labeled with the superscript '@4Fe4S'. Electronic energies of reactions involving the reduced tyrosine side chain are given in kJ/mol relative to the substrate **4**. We label iron sites with excess alpha spin density in orange and with excess beta spin density in green. SAM-derived dAdo• was used as the H-acceptor for the **4** to **R1** and **R2** to **P** + **5** oxidation steps. Empirical evidence now implicates only one SAM cosubstrate in the splicing reaction, i.e., for the initial H-abstraction (see Figure 4a); however, the use of other H-acceptors is not expected to alter the overall electronic energy trends.

water to give 4-hydroxymandelonitrile **11**, which degrades to the authenticated 4-hydroxybenzaldehyde **7** and a proposed cyanide anion would only occur with the oxidized quinone methide side chain $\mathbf{P_{ox}}$, as shown in Figure 6a. In summary, our quantum chemical analysis supports that ketoamide formation could proceed through intermediates **R1** and **R2** without thermodynamic constraints under standard conditions in the presence of a [4Fe–4S] catalyst.

Conclusion

Here we established the Pcp spliceotide pathway as a model system for detailed in vitro studies to reveal a mechanistic proposal for the extraordinary conversion of standard α-amino acids to α-keto-β^3-amino acids in peptide substrates by rSAM spliceases. Our former mechanistic hypothesis[8] had paralleled catalysis by the rSAM enzyme HydG, which acts on a tyrosine substrate to produce the CN^- ligand of the [FeFe]-hydrogenase organometallic H-cluster.[42] We reasoned that ketoamide formation by spliceases would likewise involve dissociation at Cα–Cβ to give *p*-cresol and a dehydroglycine intermediate, which would undergo CN^- extrusion to yield the spliced ketoamide—possibly initiated by H-abstraction at the analogous amino group of tyrosine (Figure S23). Unexpectedly, deuterium labeling experiments and identification of D-Tyr as the isomeric shunt **6** in this study showed that initial H-abstraction occurs predominantly at the Cα of Tyr15 in PcpA, thus necessitating a new mechanistic hypothesis.

Some other RiPP-modifying rSAM enyzmes are also known to initiate H-abstraction at the Cα of peptide residues. These include proteusin[43,44] and epipeptide[45] epimerases that convert L-amino acids to D-amino acids, sactipeptide maturases that form S–Cα thioether crosslinks,[46] as well as diverse glycyl radical enzyme activases;[47] however, none of these rSAM enzymes catalyze complex peptide backbone rearrangements. PcpXY appears to use one equivalent of SAM to catalyze ketoamide formation based on the (2-^{2}H)-Tyr-PcpA reactions (Figure 4a–b, Figure S17), which exclusively formed dAdoD as the coproduct with the ketoamide at early timepoints. If SAM was utilized to abstract further hydrogens, we would have expected coproduction of unlabeled dAdoH. Although the ketoamide has the same oxidation state as the peptide substrate, the favored mechanism based on the dehydrotyrosine radical intermediate $\mathbf{R1_{ox}}$ undergoes a net four-electron oxidation, implicating both the auxiliary [4Fe–4S] clusters and external reagents in accepting the released electrons since SAM acts only as a formal two-electron oxidant. Oxidative rSAM enzymes involved in four-electron processes (for example, HemN and BioB) use two equivalents of SAM during catalysis, whereas the majority of rSAMs that catalyze two-electron oxidations (e.g., C–C and C–S crosslinks) or even neutral reactions (e.g., epimerases) utilize one molecule of SAM.[24]

Structures of several rSAM-SPASM enzymes reveal that their peptide substrates are in proximity to the auxiliary clusters,[48–50] which could function as an electron sink during oxidative reaction steps. Multiple sequence alignments of rSAM-SPASM enzymes suggest that spliceases have an open auxiliary I iron-coordination site,[8] as has also been observed for CteB[50] and MftC[51] from sactipeptide and mycofactocin biosynthesis, respectively. Our thermodynamic energy calculations support that this open site binds precursor protein radical intermediates, which undergo C–C bond formation and side-chain extrusion while coordinated to the catalyst (Figure 6c). However, we cannot rule out the use of other non-cysteine iron-ligation partners, as has been identified for some rSAM-SPASM enzymes.[52,53] Although the fate of the unpaired electrons in splicing reactions is unknown at this time, it likely involves the auxiliary [4Fe–4S] clusters as well as external redox cofactors as part of a larger catalytic system. Future experiments will focus on resolving the role of the auxiliary [4Fe–4S] clusters and the fate of the N1 and C2 of the substrate tyrosine residue proposed to be lost as CN^- to refine our mechanistic hypothesis. The unique qualities of splicease catalysis relative to described rSAM family members and the utility of their ketoamide products as orthogonal handles for protein labeling and protease-inhibiting pharmacophores reveal these enzymes as important targets for continued study.

Supporting Information

The Experimental Section, Tables S1–S18, and Figures S1–S23 are provided in the Supporting Information.

Acknowledgments

We kindly thank Prof. Dr. Dieter Seebach and the late Prof. Dr. Albert Eschenmoser (ETH Zurich) for insightful discussions. We are grateful to the Institut Pasteur for funding the collection Pasteur Cultures of Cyanobacteria (Paris, France) and to Prof. Helge Bode (Max Planck Institute for Terrestiral Microbiology) for providing the *E. coli* Δpenta strain. R. S. acknowledges support from a Gordon and Betty Moore Foundation Symbiosis in Aquatic Systems Initiative Investigator Award (GBMF9197) and a grant from the Simons Foundation (542395FY22) as part of the Principles of Microbial Ecosystems (PriME) Collaboration.

Conflict of Interest

The authors declare no conflict of interest.

Data Availability Statement

The data that support the findings of this study are available from the corresponding author upon reasonable request.

Keywords: enzyme catalysis · metalloenzymes · natural products · post-translational modification · RiPP

[1] M. Robello, E. Barresi, E. Baglini, S. Salerno, S. Taliani, F. D. Settimo, *J. Med. Chem.* **2021**, *64*, 3508–3545.

[2] A. Arasappan, F. Bennett, S. L. Bogen, S. Venkatraman, M. Blackman, K. X. Chen, S. Hendrata, Y. Huang, R. M. Huelgas, L. Nair, A. I. Padilla, W. Pan, R. Pike, P. Pinto, S. Ruan, M. Sannigrahi, F. Velazquez, B. Vibulbhan, W. Wu, W. Yang, A. K. Saksena, V. Girijavallabhan, N.-Y. Shih, J. Kong, T. Meng, Y. Jin, J. Wong, P. McNamara, A. Prongay, V. Madison, J. J. Piwinski, K.-C. Cheng, R. Morrison, B. Malcolm, X. Tong, R. Ralston, F. G. Njoroge, *ACS Med. Chem. Lett.* **2010**, *1*, 64–69.

[3] L. Zhang, D. Lin, Y. Kusov, Y. Nian, Q. Ma, J. Wang, A. von Brunn, P. Leyssen, K. Lanko, J. Neyts, A. de Wilde, E. J. Snijder, H. Liu, R. Hilgenfeld, *J. Med. Chem.* **2020**, *63*, 4562–4578.

[4] N. Fusetani, T. Sugawara, S. Matsunaga, H. Hirota, *J. Am. Chem. Soc.* **1991**, *113*, 7811–7812.

[5] M. Kimura, T. Wakimoto, Y. Egami, K. C. Tan, Y. Ise, I. Abe, *J. Nat. Prod.* **2012**, *75*, 290–294.

[6] A. Plaza, K. Viehrig, R. Garcia, R. Müller, *Org. Lett.* **2013**, *15*, 5882–5885.

[7] M. Issac, M. Aknin, A. Gauvin-Bialecki, N. De Voogd, A. Ledoux, M. Frederich, Y. Kashman, S. Carmeli, *J. Nat. Prod.* **2017**, *80*, 1110–1116.

[8] B. I. Morinaka, E. Lakis, M. Verest, M. J. Helf, T. Scalvenzi, A. L. Vagstad, J. Sims, S. Sunagawa, M. Gugger, J. Piel, *Science* **2018**, *359*, 779–782.

[9] J. B. Broderick, B. R. Duffus, K. S. Duschene, E. M. Shepard, *Chem. Rev.* **2014**, *114*, 4229–4317.

[10] T. A. Scott, M. Verest, J. Farnung, C. C. Forneris, S. L. Robinson, X. Ji, F. Hubrich, C. Chepkirui, D. U. Richter, S. Huber, P. Rust, A. B. Streiff, Q. Zhang, J. W. Bode, J. Piel, *Chem* **2022**, *8*, 2659–2677.

[11] W. Zeng, Y. Song, R. Wang, R. He, T. Wang, *J. Pharm. Anal.* **2023**, *13*, 355–366.

[12] E. Lakis, S. Magyari, J. Piel, *Angew. Chem. Int. Ed. Engl.* **2022**, *61*, e202202695.

[13] D. Richter, E. Lakis, J. Piel, *Nat. Chem.* **2023**, *15*, 1422–1430.

[14] M. Montalbán-López, T. A. Scott, S. Ramesh, I. R. Rahman, A. J. van Heel, J. H. Viel, V. Bandarian, E. Dittmann, O. Genilloud, Y. Goto, M. J. Grande Burgos, C. Hill, S. Kim, J. Koehnke, J. A. Latham, A. J. Link, B. Martínez, S. K. Nair, Y. Nicolet, S. Rebuffat, H.-G. Sahl, D. Sareen, E. W. Schmidt, L. Schmitt, K. Severinov, R. D. Süssmuth, A. W. Truman, H. Wang, J.-K. Weng, G. P. van Wezel, Q. Zhang, J. Zhong, J. Piel, D. A. Mitchell, O. P. Kuipers, W. A. van der Donk, *Nat. Prod. Rep.* **2021**, *38*, 130–239.

[15] B. M. Hoffman, W. E. Broderick, J. B. Broderick, *Annu. Rev. Biochem.* **2023**, *92*, 333–349.

[16] T. A. J. Grell, P. J. Goldman, C. L. Drennan, *J. Biol. Chem.* **2015**, *290*, 3964–3971.

[17] N. D. Lanz, S. J. Booker, *Biochim. Biophys. Acta* **2015**, *1853*, 1316–1334.

[18] D. H. Haft, M. K. Basu, D. A. Mitchell, *BMC Biol.* **2010**, *8*, 70.

[19] B. J. Burkhart, G. A. Hudson, K. L. Dunbar, D. A. Mitchell, *Nat. Chem. Biol.* **2015**, *11*, 564–570.

[20] R. W. Castenholz, *Life* **2015**, *5*, 332–347.

[21] S. Frey, D. Görlich, *J. Chromatogr. A* **2014**, *1337*, 95–105.

[22] D. Richter, A. Courvoisier-Clément, A. L. Vagstad, S. Magyari, J. Piel, *Chem. Sci.* **2024**, *15*, 16645–16650.

[23] P. G. Arnison, M. J. Bibb, G. Bierbaum, A. A. Bowers, T. S. Bugni, G. Bulaj, J. A. Camarero, D. J. Campopiano, G. L. Challis, J. Clardy, P. D. Cotter, D. J. Craik, M. Dawson, E. Dittmann, S. Donadio, P. C. Dorrestein, K.-D. Entian, M. A. Fischbach, J. S. Garavelli, U. Göransson, C. W. Gruber, D. H. Haft, T. K. Hemscheidt, C. Hertweck, C. Hill, A. R. Horswill, M. Jaspars, W. L. Kelly, J. P. Klinman, O. P. Kuipers, A. J. Link, W. Liu, M. A. Marahiel, D. A. Mitchell, G. N. Moll, B. S. Moore, R. Müller, S. K. Nair, I. F. Nes, G. E. Norris, B. M. Olivera, H. Onaka, M. L. Patchett, J. Piel, M. J. T. Reaney, S. Rebuffat, R. P. Ross, H.-G. Sahl, E. W. Schmidt, M. E. Selsted, K. Severinov, B. Shen, K. Sivonen, L. Smith, T. Stein, R. D. Süssmuth, J. R. Tagg, G.-L. Tang, A. W. Truman, J. C. Vederas, C. T. Walsh, J. D. Walton, S. C. Wenzel, J. M. Willey, W. A. van der Donk, *Nat. Prod. Rep.* **2013**, *30*, 108–160.

[24] M. W. Ruszczycky, A. Zhong, H. Liu, *Nat. Prod. Rep.* **2018**, *35*, 615–621.

[25] A. Liu, A. Gräslund, *J. Biol. Chem.* **2000**, *275*, 12367–12373.

[26] H. Rupp, K. K. Rao, D. O. Hall, R. Cammack, *Biochim. Biophys. Acta* **1978**, *537*, 255–269.

[27] E. Panufnik, M. Kańska, *J. Labelled Compd. Radiopharm.* **2007**, *50*, 85–89.

[28] C. Kegler, F. I. Nollmann, T. Ahrendt, F. Fleischhacker, E. Bode, H. B. Bode, *ChemBioChem* **2014**, *15*, 826–828.

[29] K. Fujii, Y. Ikai, H. Oka, M. Suzuki, K. Harada, *Anal. Chem.* **1997**, *69*, 5146–5151.

[30] X. X. Han, R. S. Rodriguez, C. L. Haynes, Y. Ozaki, B. Zhao, *Nat. Rev. Methods Primers* **2022**, *1*, 1–17.

[31] C. Lacroix, E. Saussereau, F. Boulanger, J. P. Goullé, *J. Anal. Toxicol.* **2011**, *35*, 143–147.

[32] J. M. Storey, W. C. Andersen, A. Heise, S. B. Turnipseed, J. Lohne, T. Thomas, M. Madson, *Food Addit. Contam. Part A* **2015**, *32*, 657–664.

[33] K. Yea, S. Lee, J. B. Kyong, J. Choo, E. K. Lee, S.-W. Joo, S. Lee, *Analyst* **2005**, *130*, 1009–1011.

[34] C.-S. Phan, L. Chang, T. Q. N. Nguyen, A. F. L. Suarez, X. H. Ho, H. Chen, I. Y. F. Koh, B. I. Morinaka, *ACS Chem. Biol.* **2024**, *19*, 855–860.

[35] S. Guo, S. Wang, S. Ma, Z. Deng, W. Ding, Q. Zhang, *Nat. Commun.* **2022**, *13*, 2361.

[36] Abraham. Patchornik, Mordechai. Sokolovsky, *J. Am. Chem. Soc.* **1964**, *86*, 1206–1212.

[37] R. C. Bateman, W. W. Youngblood, W. H. Busby, J. S. Kizer, *J. Biol. Chem.* **1985**, *260*, 9088–9091.

[38] I. J. MacFarlane, E. M. Lees, E. E. Conn, *J. Biol. Chem.* **1975**, *250*, 4708–4713.

[39] M. E. Gallagher, S. G. Mayhew, J. P. Malthouse, M. F. Fillat, *Biochem. Soc. Trans.* **1996**, *24*, 40S.

[40] D. Chen, R. Scopelliti, X. Hu, *J. Am. Chem. Soc.* **2010**, *132*, 928–929.

[41] L. Noodleman, *Inorg. Chem.* **1991**, *30*, 246–256.

[42] R. D. Britt, L. Tao, G. Rao, N. Chen, L.-P. Wang, *ACS Bio. Med. Chem. Au* **2021**, *2*, 11–21.

[43] A. L. Vagstad, T. Kuranaga, S. Püntener, V. R. Pattabiraman, J. W. Bode, J. Piel, *Angew. Chem. Int. Ed. Engl.* **2019**, *58*, 2246–2250.

[44] W. G. Walls, A. L. Vagstad, T. Delridge, J. Piel, W. E. Broderick, J. B. Broderick, *J. Am. Chem. Soc.* **2024**, *146*, 5550–5559.

[45] A. Benjdia, A. Guillot, P. Ruffié, J. Leprince, O. Berteau, *Nat. Chem.* **2017**, *9*, 698–707.

[46] A. Benjdia, A. Guillot, B. Lefranc, H. Vaudry, J. Leprince, O. Berteau, *Chem. Commun.* **2016**, *52*, 6249–6252.

[47] L. R. F. Backman, M. A. Funk, C. D. Dawson, C. L. Drennan, *Crit. Rev. Biochem. Mol. Biol.* **2017**, *52*, 674–695.

[48] P. J. Goldman, T. L. Grove, L. A. Sites, M. I. McLaughlin, S. J. Booker, C. L. Drennan, *Proc. Natl. Acad. Sci. USA* **2013**, *110*, 8519–8524.

[49] K. M. Davis, K. R. Schramma, W. A. Hansen, J. P. Bacik, S. D. Khare, M. R. Seyedsayamdost, N. Ando, *Proc. Natl. Acad. Sci. USA* **2017**, *114*, 10420–10425.
[50] T. L. Grove, P. M. Himes, S. Hwang, H. Yumerefendi, J. B. Bonanno, B. Kuhlman, S. C. Almo, A. A. Bowers, *J. Am. Chem. Soc.* **2017**, *139*, 11734–11744.
[51] R. Ayikpoe, T. Ngendahimana, M. Langton, S. Bonitatibus, L. M. Walker, S. S. Eaton, G. R. Eaton, M.-E. Pandelia, S. J. Elliott, J. A. Latham, *Biochemistry* **2019**, *58*, 940–950.
[52] W. Zhu, L. M. Walker, L. Tao, A. T. Iavarone, X. Wei, R. D. Britt, S. J. Elliott, J. P. Klinman, *J. Am. Chem. Soc.* **2020**, *142*, 12620–12634.
[53] Y. Lien, J. C. Lachowicz, A. Mendauletova, C. Zizola, T. Ngendahimana, A. Kostenko, S. S. Eaton, J. A. Latham, T. L. Grove, *ACS Chem. Biol.* **2024**, *19*, 370–379.

Manuscript received: September 19, 2024
Accepted manuscript online: December 17, 2024
Version of record online: ■■, ■■

Research Article

Enzyme Catalysis

A. L. Vagstad,* E. Lakis, K.-S. Csizi, W. Walls, D. Richter, K. Soo Lee, R. Stocker, M. Gugger, W. E. Broderick, J. B. Broderick, M. Reiher, J. Piel* **e202418054**

Mechanistic Insights Into Post-Translational α-Keto-β-Amino Acid Formation by a Radical *S*-Adenosyl Methionine Peptide Splicease

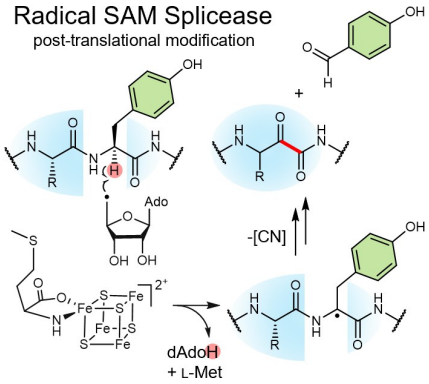

Noncanonical protein splicing illuminated: Radical *S*-adenosyl methionine spliceases post-translationally install α-keto-β-amide residues in a widespread family of peptide natural products. Here, we established the in vitro activity of a model splicease to interrogate its mechanism. The key data establish tyrosine Cα as the initial site of peptide radical formation and 4-hydroxybenzaldehyde as the tyrosine-derived coproduct to instruct our mechanistic proposal to this protease-inhibiting pharmacophore.